Title

Cryo-EM Elucidation of the Structure of Bacteriophage P22 Virions after Genome Release

Journal

Biophysical Journal, 114(6)

ISSN

0006-3495

Authors

McNulty, Reginald
Cardone, Giovanni
Gilcrease, Eddie B
et al.

Publication Date

2018-03-01

DOI

10.1016/j.bpj.2018.01.026

Peer reviewed

Biophysical Journal
Article

Biophysical Society

Cryo-EM Elucidation of the Structure of Bacteriophage P22 Virions after Genome Release

Reginald McNulty,[1,*] Giovanni Cardone,[2] Eddie B. Gilcrease,[4] Timothy S. Baker,[2,3] Sherwood R. Casjens,[4] and John E. Johnson[5,*]

[1]Laboratory of Gene Regulation and Signal Transduction, Department of Pharmacology, School of Medicine, University of California, San Diego, La Jolla, California; [2]Department of Chemistry and Biochemistry and [3]Division of Biological Sciences, University of California, San Diego, La Jolla, California; [4]Division of Microbiology and Immunology, Pathology Department, University of Utah School of Medicine, Salt Lake City, Utah; and [5]Department of Integrative Structural and Computational Biology, The Scripps Research Institute, La Jolla, California

ABSTRACT Genome ejection proteins are required to facilitate transport of bacteriophage P22 double-stranded DNA safely through membranes of *Salmonella*. The structures and locations of all proteins in the context of the mature virion are known, with the exception of three ejection proteins. Furthermore, the changes that occur to the proteins residing in the mature virion upon DNA release are not fully understood. We used cryogenic electron microscopy to obtain what is, to our knowledge, the first asymmetric reconstruction of mature bacteriophage P22 after double-stranded DNA has been extruded from the capsid—a state representative of one step during viral infection. Results of icosahedral and asymmetric reconstructions at estimated resolutions of 7.8 and 12.5 Å resolutions, respectively, are presented. The reconstruction shows tube-like protein density extending from the center of the tail assembly. The portal protein does not revert to the more contracted, procapsid state, but instead maintains an extended and splayed barrel structure. These structural details contribute to our understanding of the molecular mechanism of P22 phage infection and also set the foundation for future exploitation serving engineering purposes.

INTRODUCTION

Genome ejection by tailed DNA bacteriophages is a complex process about which limited molecular and structural details are known (1). The double-stranded DNA bacteriophages carry one of three types of tail: long contractile (members of the family *Myoviridae*), long noncontractile (*Siphoviridae*), and short noncontractile (*Podoviridae*). Although the very substantial tail contraction during *Myoviridae* DNA delivery into the host cell is best understood (2–5), the apparently subtler changes in long and short noncontractile tails during this process are less clear (1,6). In addition to structural protein rearrangements, DNA ejection is accompanied by the release of a few proteins. These "ejection proteins" may prepare the host cytoplasm for DNA arrival (7–9) or physically aid the transfer of the DNA through the host membranes and/or periplasmic space (10,11). In this article, we compare the structures of the short-tailed phage P22 virion before and after DNA release.

P22 is a member of the family *Podoviridae* that infects *Salmonella enterica*. Like other tailed phages, P22 virions assemble by first building a protein procapsid, into which the genome is subsequently packaged (12,13). The spherical procapsid is composed of six proteins: major capsid protein (gene product 5 or gp5), portal protein (gp1), scaffolding protein (gp8), and three "ejection proteins" (gp7, gp16, and gp20). Virion assembly then proceeds when the genome packaging motor complex gp2/gp3 binds to the procapsid (14). The gp3 subunit recognizes the DNA to be packaged (15), and gp2 uses ATP hydrolysis as an energy source to insert the DNA into the procapsid at high density (16). DNA is packaged by a "headful" mechanism, and the nuclease domain of gp2 cleaves the packaged DNA from the rest of the concatemeric DNA substrate (17). DNA packaging also results in rearrangement of the hexons (hexamers of gp5) in the capsid (18,19), loss of scaffolding protein (20), and sequential binding of tail proteins gp4 and gp10 (21,22). The mature virion is then completed by the addition of 18 copies of the tailspike protein (gp9) (23), and the genome is sealed inside the head by the addition of a trimer of gp26 needle proteins that plugs the channel employed by the DNA to enter the procapsid (22,24).

Cryogenic electron microscopy (cryo-EM) reconstructions of the asymmetric P22 mature virion (25–28) have allowed the placement of all the virion proteins in the

Submitted August 3, 2017, and accepted for publication January 17, 2018.

*Correspondence: rmcnulty@ucsd.edu or jackj@scripps.edu

Editor: Andreas Engel.

https://doi.org/10.1016/j.bpj.2018.01.026

structure with the exception of the three ejection proteins, as these are lost from the virion and presumed to be released with the DNA during ejection. Although all three proteins are required for successful DNA release into the target cell (29,30), they are not required for the assembly of apparently normal-appearing virions (13,31–33). Density first tentatively assigned to the ejection proteins (27) was later found to be at least largely attributed to the C-terminal "barrel" of the portal protein (34). Ejection proteins have been indirectly located near the center of the head by the bubblegram imaging method (35), but details of their location are not known.

Though most proteins in tailed bacteriophages remain on the outside of the host cell during bacterial infection, these phages have evolved efficient mechanisms to ensure their genome is safely delivered to the bacterial cytoplasm. For phages such as P22 that infect Gram-negative hosts, the genome must traverse the outer cell membrane, peptidoglycan layer, periplasmic space, and inner membrane to reach the cytoplasm. DNA delivery by short-tailed phages is poorly understood, and the roles of the ejection proteins remain unclear. Low-resolution tomographic reconstructions of phage T7 virions at various stages of DNA ejection reveal the assembly of an apparent tube that extends away from the virion along the portal axis through the periplasm (10). This tube may serve as a conduit for delivery of the DNA into the cytoplasm (1,10), and T7 proteins gp14, gp15, and gp16 appear to be involved in this transport, but their specific roles in this process remain unclear (11,36). P22 and T7 are very different in the assembly mechanism of tail- and core-associating proteins (37), and the ejection proteins of the two phages exhibit no sequence homology. One of the ejection proteins of the P22-like phage Sf6 (a P22 gp20 homolog) self-assembles in vitro into tubes that could be involved in transport of the DNA through the periplasm (38).

The precise cell-contact signal that causes the P22 virion to release its DNA during the process of delivery of the DNA into a target cell is not known. One hypothesis is that the peptide linker between the tailspike protein's particle (capsid) binding domain and its receptor binding domain relays the signal of phage-receptor binding sensed by the tailspike (39). Another hypothesis is that penetration of the gp26 needle into the outer membrane triggers the release of the ejection proteins and genome (40). The C-terminal domain of the gp26 needle plugs the phage chromosome's exit channel (40,41), and in gp26 deletion mutants, P22 virion assembly and DNA packaging occur normally, but the packaged DNA is unstable and spontaneously leaks out of these particles (41,42). The resulting empty particles—which lack gp26 and DNA and are sometimes called "empty heads"—contain coat protein, portal protein, tailspike protein, and all three ejection proteins (13,43). Low-resolution tomographic structures of *Escherichia coli* phages P1 (2) and T4 (44), cyanophage Syn5 (45), and *Bacillus subtilis* phage ø29 (46) bound to their target bacteria have been determined; however, there are no published high-resolution cryo-EM structures of bacteriophages that have ejected their DNA. Here, we use cryo-EM to study the structural differences between intact P22 virions and particles that have lost their DNA.

MATERIALS AND METHODS

Preparation of empty P22 particles

S. enterica LT2 strain DB7000 (47) was grown in 0.5 L of LB broth at 37°C to 2 × 10^8 cells/mL and infected with seven P22 c1-7, *26*$^{-}$*am*H204, *13*$^{-}$*am*H101 (48) phage per cell (this phage was propagated for this infection on host strain DB7004 (47)). After 120 min of shaking at 37°C, cells were pelleted, resuspended in 10 mL LB broth, and lysed by shaking with 0.2 mL chloroform. The concentrated lysate was treated briefly with 1 μg/mL DNase I at room temperature to reduce viscosity, and cell debris was removed by centrifugation at 5000 revolutions per minute (Rpm) in an Eppendorff A-44-4 rotor for 20 min. The supernatant was applied to several CsCl step gradient tubes (49) and spun in a Beckman SW41 rotor at 36,000 Rpm for 2 h, and the visible band at 1.4 gm/cc density was harvested by needle puncture. The sample was dialyzed against TM buffer (10 mM Tris-Cl, 1 mM MgCl2, (pH 7.4)), loaded onto four SW41 rotor tubes that contained a 5–20% sucrose gradient in TM buffer. The visible opalescent empty particle band was harvested by needle puncture. The empty particle fraction was concentrated ~10-fold with an Amicon Ultra centrifugal filter, dialyzed against TM buffer, further purified by a second identical sucrose gradient velocity sedimentation, again harvested by needle puncture, and dialyzed against TM buffer.

Cryo-EM data collection and image processing

The empty particle sample was screened for homogeneity and concentration by freeze-plunging grids in liquid ethane, followed by inspection in an FEI Talos transmission electron microscope (FEI, Hillsboro, OR) operated at 200 KeV. Ice thickness and sample concentration over the grid holes were optimized by adjusting the blot time and visual inspection at the microscope. Micrographs were acquired in nanoprobe mode at a nominal magnification of 92,000× (pixel size of 0.158 nm) with an FEI Falcon 2 4K × 4K direct detector camera (FEI) and a defocus range between −1 and −3 μm. Grid areas were targeted using Leginon (50). A dose of 12 e^{-}/pix/s was applied for 12 s for a total dose of 57.6 $e^{-}/Å^2$. Acquired images consisted of 30 frames corresponding to 400 ms per frame.

Reconstruction was performed using the single-model refinement pipeline in Appion (51). The icosahedral, mature virus protein data bank (PDB) model 2XYZ (18) was low-pass-filtered to 50 Å and used as an initial model. Appion was used to prepare all initial parameter files for Frealign refinement. An initial global alignment was performed in Frealign (mode 3) until no further improvement of resolution was obtained. Subsequently, refinement (mode 1) proceeded until no improvement in resolution was obtained. An initial model was also prepared using ab initio methods in Auto3DEM (Baker Lab Software, La Jolla, CA), in which only the particles are utilized to produce the model. Refinement of this model in Auto3DEM reached a resolution similar to that obtained with Frealign.

The Frealign icosahedral reconstruction was low-pass-filtered to 50 Å, which allowed visualization of a low-resolution, low-intensity tail positioned at each of the 12 fivefold vertices. Using commands in BSOFT and Chimera (UCSF), an asymmetric model was constructed by computationally enhancing the tail from just one fivefold vertex of the icosahedral reconstruction. Refinement in Auto3DEM proceeded first by limiting the

search to the 60 equivalent icosahedral orientations (mode TICOS_equiv) obtained during the symmetric reconstruction to determine which one would agree with the asymmetric model. Subsequent refinement was performed using gold-standard criteria (i.e., the data were split and refined independently until the two maps converged upon a single model). The portal protein density was obtained from the empty particles in a way similar to molecular replacement crystallography (52); the proper alignment of the particles to the initial model—which consisted of only capsid and tail—enabled appearance of the portal protein density at the same fivefold vertex. To enhance protein density in the tail and portal regions for visualization purposes, the final asymmetric model was first oriented with the tail aligned to the Z axis. Subsequently, sixfold symmetry was imposed to visualize density in the tail region, and 12-fold symmetry was used to analyze density in the portal region. The local resolutions of the icosahedral and asymmetric reconstructions were analyzed using the e2FSC.py feature in EMAN2 (53). Icosahedral and asymmetric reconstructions have been deposited to the Electron Microscopy Data Bank (EMDB) under entries EMDB: 7315, EMDB: 7316 (C6 along Z axis), and EMDB: 7317 (C12 along Z axis).

RESULTS

Visualization of gp26$^-$ P22 particles by cryo-EM

Empty phage P22 particles were prepared by infecting *S. enterica* with P22 phages carrying a null nonsense mutation in gene 26 and purifying the resulting particles by density and velocity centrifugation (see Materials and Methods). Examination of the proteins present in these particles by SDS gel electrophoresis agrees with previous studies showing that, except for gp26, all the P22 virion proteins are present, including the three ejection proteins (13,33). Our more recent analyses have shown that the three ejection proteins are all present in the same number of copies (within experimental error) in mature virions and 26$^-$ empty heads (Fig. S1). Grids with these particles were prepared and examined by cryo-EM. The resulting images revealed particles in various orientations and contained views of both the capsid and tail proteins (Fig. 1). It was evident that no DNA was present inside the particles, which were marked by the absence of genome density that was observed in reconstructions of mature virions (26). Unexpectedly, the phages had elongated structure features with a surfboard-like morphology attached to many of their tails. These "surfboards" were only observed in gp26$^-$ particles (i.e., those lacking the needle); they were not seen in preparations of native virions. Nonetheless, it remains possible that they consist of pieces of bacterial membrane/peptidoglycan that copurify with the particles.

Icosahedral cryo-EM reconstruction of gp26$^-$ P22 empty particles

Reconstruction of the empty P22 particles was performed as follows: 200 micrographs recorded at a nominal magnification of 92,000× were processed using the Appion software pipeline (51). A total of 1935 particle images were manually picked using e2boxer (53), and defocus estimation was performed with CTFFIND4 (54). An icosahedral reconstruction of P22 (55), low-pass-filtered to 50 Å, was used as an initial model for refinement with Frealign (56). A reconstruction with icosahedral symmetry was determined and refined to 7.8 Å resolution (0.143 FSC threshold criterion (57)) (Fig. S2). As expected, this reconstruction reveals a capsid structure in which the gp5 coat proteins adopt the same T = 7 laevo arrangement as found in mature P22 virions, and prominent secondary structure features of the coat protein were discernible. By imposing icosahedral symmetry in the reconstruction process, densities for the portal vertex and the tail structure are smeared out by a factor of 12-fold with the remaining 11 identical fivefold vertices. To examine differences among the seven coat proteins (*A–G*) that make up the icosahedral asymmetric unit, an atomic model (PDB: 2XYZ) (18) of the mature virion coat protein was docked as a rigid body into density for each of the seven uniquely positioned subunits using Chimera (58) (Fig. 2). At this resolution, subunits (Fig. 2, *A–F*) do not display detectable differences in monomer shape or intramolecular organization compared to the mature virion. However, density was significantly displaced in the volume corresponding to the spine helix for fivefold proximal G subunits when compared to the mature virion (*red arrow* in Fig. 2). The overall shape of the empty particle is indistinguishable from that of the intact mature virion, indicating that the lack of internal "DNA pressure" in the

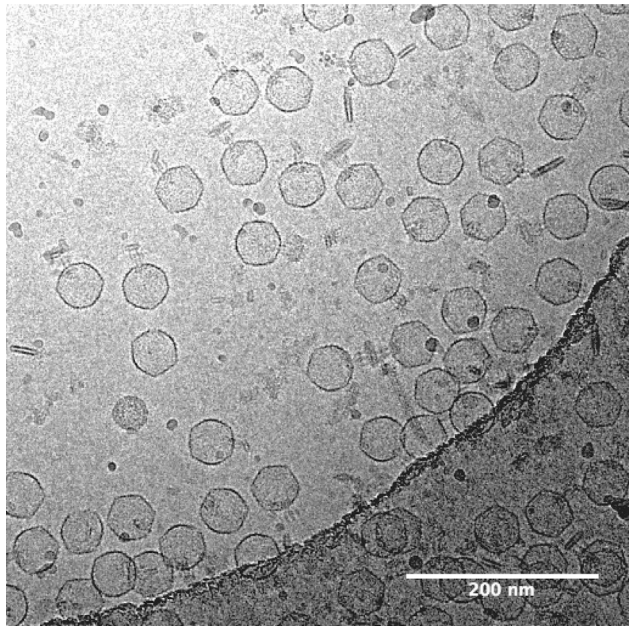

FIGURE 1 Representative cryo-EM micrograph of gp26$^-$ empty P22 particles. An FEI Talos microscope operating at 200 KeV was used to image P22 empty particles at defocus settings ranging between −1 and −3 μm underfocus. Micrographs were acquired with nanoprobe mode at a nominal magnification of 92,000× (pixel size of 0.158 nm) and spot index six with a 4K × 4K FEI Falcon two-direct detector camera and a total dose of ~57.6 e^-/A^2. The scale bar represents 200 nm.

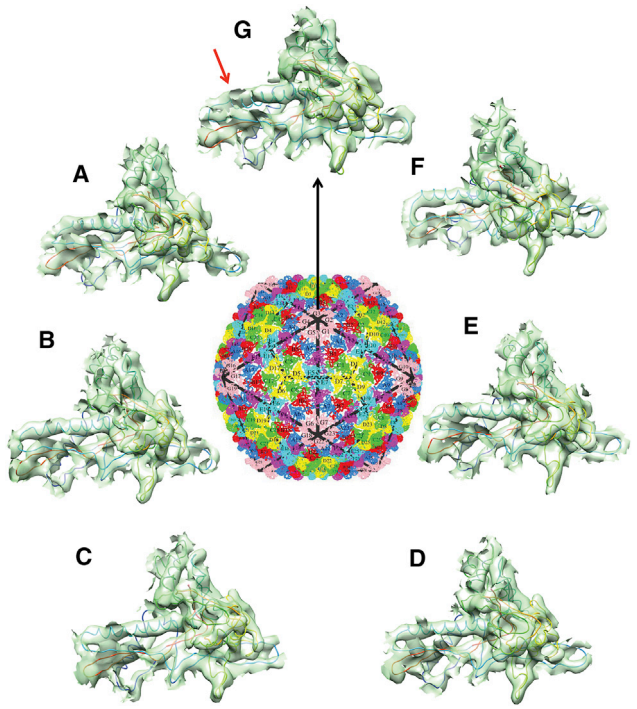

FIGURE 2 Analysis of density changes in the empty P22 particle asymmetric unit. PDB: 2XYZ (*colored rainbow*) was rigid-body docked into the density for each of the seven gp5 subunits (*A–G*) in each icosahedral asymmetric unit. Changes were observed in the spine helix of subunit (*G*) (*red arrow*) as evidenced by the model residing outside of the density envelope. In the middle is the icosahedral model PDB: 2XYZ enclosed inside an icosahedral cage (*black*). Molecules in each asymmetric unit are color-coded to distinguish among the seven subunits (those at each vertex are colored pink). To see this figure in color, go online.

empty particles does not cause the sides of the particle to deform. The intersubunit interactions of the N-terminal coat protein helices and P-loop are sufficiently strong and inflexible to prevent particle deformation (19).

Asymmetric cryo-EM reconstruction of gp26$^-$ P22 empty particles

Since each particle contains only one tail at a unique five-fold vertex, application of icosahedral symmetry forces all vertices to be equivalent because density for the single tail is averaged together with the density (or lack of density) at all 12 vertices. To produce an asymmetric reconstruction that retains the full signal for the portal and tail protein densities, the icosahedral map was low-pass-filtered to 50 Å, the resolution at which it displays replicates of the tail density at one-twelfth its original strength at each of the 12 vertices. An initial asymmetric model was made by isolating the tail density from a single fivefold vertex and appending it to one vertex of the icosahedral-symmetrized model using commands in BSOFT (12) and Chimera (58). This asymmetric model was initially refined in Auto3DEM (ticos_equiv mode) (59) by probing the 60 orientations equivalent to the ones previously obtained for each particle. Subsequently, Auto3DEM was used also for the gold-standard (57) local refinement procedure. BSOFT scripts were used to orient the asymmetric reconstruction with its tail aligned to the Z axis, followed by imposing either C6 or C12 symmetry to enhance the density associated with the hexameric tail or the dodecameric portal protein, respectively.

The reconstructed gp26$^-$ P22 empty particle (Fig. 3) was determined at an overall resolution of 12.5 Å as determined using the FSC cutoff 0.143 (Fig. S3). Analysis of the asymmetric reconstruction with e2fsc.py in EMAN2 (53) shows local resolutions ranging between 11 and 20 Å for portal and tail machine densities, whereas the capsid was resolved at 11 Å (Fig. S4). The asymmetric capsid was determined at a significantly lower overall resolution (~11 Å) compared to the icosahedrally symmetrized capsid (~7.8 Å). The lower resolution observed in the portal-tail vicinity could be a consequence of the averaging power changing from icosahedral (60-fold) to asymmetric (onefold).

As expected, the reconstruction of the gp26$^-$ particle is missing the gp26 needle that seals the DNA inside the phage, and the inside of the capsid does not contain the density previously assigned to DNA in the virion (26). Strikingly, a short hollow tube that is not present in mature virions extends from gp10 at the base of the tail along the tail axis (Fig. 3; *black arrow*). When C6 symmetry is applied to the tail portion of the density map, the hollow tube is only resolved to ~20 Å, but the six copies of gp10 located just above this region are resolved at ~10 Å resolution (Fig. S4). This suggests the density extending from gp10 is distinct. The possible origin of this unique density is discussed below.

The portal protein density was reconstructed from the empty particles in a way similar to molecular replacement crystallography (52); the model used to initiate the asymmetric reconstruction process contained a 50 Å, low-pass-filtered model of just the tail and capsid. Density for

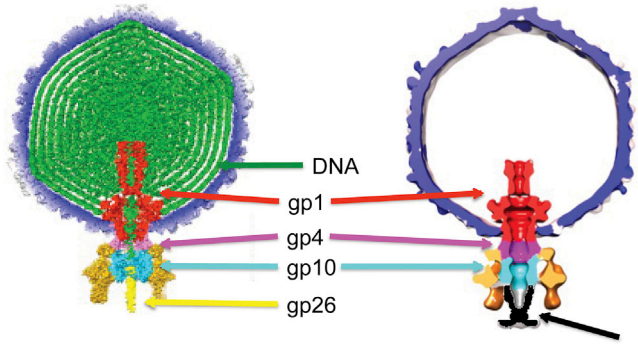

FIGURE 3 Comparison of mature WT P22 (26) (*left*) and empty P22 particle (*right*) asymmetric reconstructions. The empty P22 particle reconstruction is missing DNA (*green*) and the gp26 plug (*yellow*). The new density (*black arrow*) is found in the empty P22 particle extending from gp10 (*cyan*). To see this figure in color, go online.

the portal protein subsequently appeared after refinement. This method also reduced model bias because the starting asymmetric model originated directly from the data that was not initially visible in the icosahedral reconstruction, and in addition, evidence for portal density was apparent. An atomic model of portal protein from the mature virion (PDB: 5JJ3 (55)) was docked into the corresponding three-dimensional density of the empty particle reconstruction using the fit map feature in Chimera (Fig. 4). The empty particle portal was found to be indistinguishable from the virion portal at this resolution, except that the C-terminal barrel portion of the dodecameric portal is splayed at the top relative to the virion model (Fig. 4). When C12 symmetry was applied to the portal protein portion of the density map, the resolution of features in the portal protein ranged between 8 and 20 Å (Fig. S4).

DISCUSSION

To our knowledge, we report the first cryo-EM asymmetric reconstruction of bacteriophage P22 after it has released its packaged double-stranded DNA chromosome. The phage P22 portal protein is known to have different conformations depending on the maturation state of the virus (55), but it remained plausible that the conformation of the portal protein might have an additional change in empty particles since interactions with DNA would be lost upon genome ejection. Could the portal C-terminal barrel invert to extend through the tail and be the protective structure that delivers the genome through the protective barriers of *Salmonella*? Here, our results demonstrate that the portal structure remains essentially unchanged inside the capsid after DNA release and does not revert to the conformation it adopts in procapsids. It does, however, undergo a conformational change with respect to the conformation observed in mature virions, with the top of the C-terminal barrel appearing to be splayed out in the empty particle. These conformational changes in the fivefold vertex occur in the portal and tail machine.

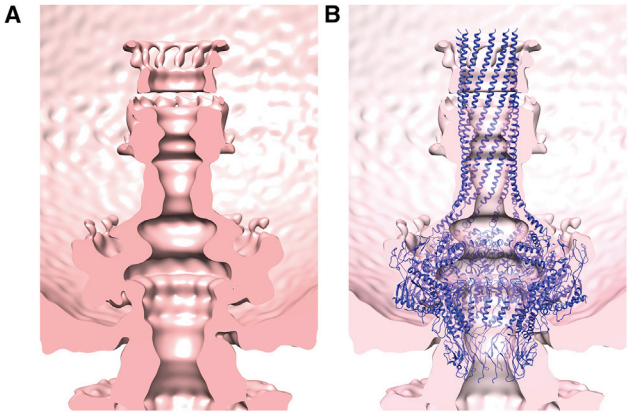

FIGURE 4 Comparison of portal protein conformation found in mature virus and empty P22 particles. (*A*) shows the density of portal protein from empty P22 particles. (*B*) shows the rigid-body docking of portal protein PDB: 5JJ3 (*blue*) in empty P22 particles (*pink*). Density at the portal barrel apex is splayed in the empty P22 particle compared with that found in the mature DNA-filled particle (*purple*). To see this figure in color, go online.

The asymmetric reconstruction shows a substantial density, not present in virions, that extends away from gp10 at the distal tip of the short tail. This density has a tube shape that narrows and is capped off at its distal end. This density cannot be ascribed to gp26 because these particles have a premature stop at codon 53 in gene *26* (this mutation is a C to T change that creates a TAG codon from CAG; unpublished data). Moreover, SDS gel analysis of gp26$^-$ phages show they are null for the gp26 plug and that they contain all three ejection proteins (Fig. S1). The density in the reconstruction is also not affected by "surfboards," which appear in less than 10% of the particles. Digital removal of the "surfboard" density does not affect the density extruding from the phage tail, suggesting that the extra density is a real structural component of the tail (Fig. S5). Previous studies have shown that particles lacking the gp26 plug contain ejection proteins associated with them (13), and since the structures and location of all P22 virion proteins are known in the mature virus except for the three ejection proteins, we believe that this tube-like density is likely to be a remodeled form of one of these proteins (gp16, gp7, or gp20). We hypothesize that this short tube may serve as a precursor assembly in the formation of a longer tube comprised of the other ejection proteins, and the longer tube is used to deliver the virion genome into the host cytoplasm through the outer membrane, peptidoglycan layer, periplasmic space, and inner membrane. Nonhomologous proteins in the short-tailed phage T7 are also thought to form a tube, as evidenced by cryo-EM tomography of virions bound to cells (10,11,36). In our study, the gp26$^-$ empty phage particles are not attached to intact bacterial membrane, probably reducing the resolution compared to the T7 study.

All viruses have proteins that interact with a host membrane at some point during infection. Many viruses have been shown to interact with host membranes during infection and, in some cases, during maturation (60). Higher-resolution studies of viral proteins in association with membranes is key to elucidating detailed mechanisms of membrane disruption, which can ultimately be exploited for viral engineering or drug-based inhibition during disease by enabling targeting to specific membranes of different cells.

SUPPORTING MATERIAL

Five figures are available at http://www.biophysj.org/biophysj/supplemental/S0006-3495(18)30185-1.

AUTHOR CONTRIBUTIONS

S.R.C., J.E.J., and T.S.B. designed the research. R.M., E.B.G., and G.C. performed the research. R.M., G.C., J.E.J., and S.R.C. analyzed data. R.M. and S.R.C. wrote the article.

ACKNOWLEDGMENTS

R.M. was supported by National Institutes of Health grants P42ES010337-16S1 and F32 GM108310. S.C. and E.G. were supported by RO1 GM114817. G.C. and T.B. were supported in part by R01 GM033050.

REFERENCES

1. Casjens, S. R., and I. J. Molineux. 2012. Short noncontractile tail machines: adsorption and DNA delivery by podoviruses. *Adv. Exp. Med. Biol.* 726:143–179.
2. Liu, J., C. Y. Chen, …, W. Margolin. 2011. Visualization of bacteriophage P1 infection by cryo-electron tomography of tiny Escherichia coli. *Virology.* 417:304–311.
3. Taylor, N. M., N. S. Prokhorov, …, P. G. Leiman. 2016. Structure of the T4 baseplate and its function in triggering sheath contraction. *Nature.* 533:346–352.
4. Yap, M. L., T. Klose, …, M. G. Rossmann. 2016. Role of bacteriophage T4 baseplate in regulating assembly and infection. *Proc. Natl. Acad. Sci. USA.* 113:2654–2659.
5. Nováček, J., M. Šiborová, …, P. Plevka. 2016. Structure and genome release of Twort-like Myoviridae phage with a double-layered baseplate. *Proc. Natl. Acad. Sci. USA.* 113:9351–9356.
6. Davidson, A. R., L. Cardarelli, …, K. L. Maxwell. 2012. Long noncontractile tail machines of bacteriophages. *Adv. Exp. Med. Biol.* 726:115–142.
7. Bair, C. L., D. Rifat, and L. W. Black. 2007. Exclusion of glucosylhydroxymethylcytosine DNA containing bacteriophages is overcome by the injected protein inhibitor IPI*. *J. Mol. Biol.* 366:779–789.
8. Alawneh, A. M., D. Qi, …, Y. Otsuka. 2016. An ADP-ribosyltransferase Alt of bacteriophage T4 negatively regulates the Escherichia coli MazF toxin of a toxin-antitoxin module. *Mol. Microbiol.* 99:188–198.
9. Koch, T., and W. Rüger. 1994. The ADP-ribosyltransferases (gpAlt) of bacteriophages T2, T4, and T6: sequencing of the genes and comparison of their products. *Virology.* 203:294–298.
10. Hu, B., W. Margolin, …, J. Liu. 2013. The bacteriophage t7 virion undergoes extensive structural remodeling during infection. *Science.* 339:576–579.
11. Lupo, D., S. Leptihn, …, A. Kuhn. 2015. The T7 ejection nanomachine components gp15-gp16 form a spiral ring complex that binds DNA and a lipid membrane. *Virology.* 486:263–271.
12. Botstein, D., C. H. Waddell, and J. King. 1973. Mechanism of head assembly and DNA encapsulation in *Salmonella* phage p22. I. Genes, proteins, structures and DNA maturation. *J. Mol. Biol.* 80:669–695.
13. King, J., E. V. Lenk, and D. Botstein. 1973. Mechanism of head assembly and DNA encapsulation in *Salmonella* phage P22. II. Morphogenetic pathway. *J. Mol. Biol.* 80:697–731.
14. McNulty, R., R. K. Lokareddy, …, G. Cingolani. 2015. Architecture of the complex formed by large and small terminase subunits from bacteriophage P22. *J. Mol. Biol.* 427:3285–3299.
15. Casjens, S., W. M. Huang, …, R. Parr. 1987. Initiation of bacteriophage P22 DNA packaging series. Analysis of a mutant that alters the DNA target specificity of the packaging apparatus. *J. Mol. Biol.* 194:411–422.
16. Fuller, D. N., D. M. Raymer, …, D. E. Smith. 2007. Single phage T4 DNA packaging motors exhibit large force generation, high velocity, and dynamic variability. *Proc. Natl. Acad. Sci. USA.* 104:16868–16873.
17. Casjens, S., and M. Hayden. 1988. Analysis in vivo of the bacteriophage P22 headful nuclease. *J. Mol. Biol.* 199:467–474.
18. Chen, D. H., M. L. Baker, …, W. Chiu. 2011. Structural basis for scaffolding-mediated assembly and maturation of a dsDNA virus. *Proc. Natl. Acad. Sci. USA.* 108:1355–1360.
19. Parent, K. N., R. Khayat, …, T. S. Baker. 2010. P22 coat protein structures reveal a novel mechanism for capsid maturation: stability without auxiliary proteins or chemical crosslinks. *Structure.* 18:390–401.
20. King, J., and S. Casjens. 1974. Catalytic head assembling protein in virus morphogenesis. *Nature.* 251:112–119.
21. Olia, A. S., J. Al-Bassam, …, G. Cingolani. 2006. Binding-induced stabilization and assembly of the phage P22 tail accessory factor gp4. *J. Mol. Biol.* 363:558–576.
22. Olia, A. S., A. Bhardwaj, …, G. Cingolani. 2007. Role of gene 10 protein in the hierarchical assembly of the bacteriophage P22 portal vertex structure. *Biochemistry.* 46:8776–8784.
23. Israel, J. V., T. F. Anderson, and M. Levine. 1967. *In vitro* morphogenesis of phage P22 from heads and base-plate parts. *Proc. Natl. Acad. Sci. USA.* 57:284–291.
24. Berget, P. B., and A. R. Poteete. 1980. Structure and functions of the bacteriophage P22 tail protein. *J. Virol.* 34:234–243.
25. Chang, J., P. Weigele, …, W. Jiang. 2006. Cryo-EM asymmetric reconstruction of bacteriophage P22 reveals organization of its DNA packaging and infecting machinery. *Structure.* 14:1073–1082.
26. Tang, J., G. C. Lander, …, J. E. Johnson. 2011. Peering down the barrel of a bacteriophage portal: the genome packaging and release valve in p22. *Structure.* 19:496–502.
27. Lander, G. C., L. Tang, …, J. E. Johnson. 2006. The structure of an infectious P22 virion shows the signal for headful DNA packaging. *Science.* 312:1791–1795.
28. Hryc, C. F., D. H. Chen, …, W. Chiu. 2017. Accurate model annotation of a near-atomic resolution cryo-EM map. *Proc. Natl. Acad. Sci. USA.* 114:3103–3108.
29. Israel, V. 1977. E proteins of bacteriophage P22. I. Identification and ejection from wild-type and defective particles. *J. Virol.* 23:91–97.
30. Jin, Y., S. M. Sdao, …, K. N. Parent. 2015. Bacteriophage P22 ejects all of its internal proteins before its genome. *Virology.* 485:128–134.
31. Hoffman, B., and M. Levine. 1975. Bacteriophage P22 virion protein which performs an essential early function. I. Analysis of 16-ts mutants. *J. Virol.* 16:1536–1546.
32. Hoffman, B., and M. Levine. 1975. Bacteriophage P22 virion protein which performs an essential early function. II. Characterization of the gene 16 function. *J. Virol.* 16:1547–1559.
33. Poteete, A. R., and J. King. 1977. Functions of two new genes in Salmonella phage P22 assembly. *Virology.* 76:725–739.
34. Olia, A. S., P. E. Prevelige, Jr., …, G. Cingolani. 2011. Three-dimensional structure of a viral genome-delivery portal vertex. *Nat. Struct. Mol. Biol.* 18:597–603.
35. Wu, W., J. C. Leavitt, …, A. C. Steven. 2016. Localization of the houdinisome (ejection proteins) inside the bacteriophage P22 virion by bubblegram imaging. *MBio.* 7:e01152-16.
36. Chang, C. Y., P. Kemp, and I. J. Molineux. 2010. Gp15 and gp16 cooperate in translocating bacteriophage T7 DNA into the infected cell. *Virology.* 398:176–186.
37. Fokine, A., and M. G. Rossmann. 2014. Molecular architecture of tailed double-stranded DNA phages. *Bacteriophage.* 4:e28281.
38. Zhao, H., J. A. Speir, …, L. Tang. 2016. Structure of a bacterial virus DNA-injection protein complex reveals a decameric assembly with a constricted molecular channel. *PLoS One.* 11:e0149337.
39. Seul, A., J. J. Müller, …, R. Seckler. 2014. Bacteriophage P22 tailspike: structure of the complete protein and function of the interdomain linker. *Acta Crystallogr. D Biol. Crystallogr.* 70:1336–1345.
40. Bhardwaj, A., R. S. Sankhala, …, G. Cingolani. 2016. Structural plasticity of the protein plug that traps newly packaged genomes in Podoviridae virions. *J. Biol. Chem.* 291:215–226.
41. Strauss, H., and J. King. 1984. Steps in the stabilization of newly packaged DNA during phage P22 morphogenesis. *J. Mol. Biol.* 172:523–543.

42. Lenk, E., S. Casjens, …, J. King. 1975. Intracellular visualization of precursor capsids in phage P22 mutant infected cells. *Virology.* 68:182–199.

43. Casjens, S., and J. King. 1974. P22 morphogenesis. I: catalytic scaffolding protein in capsid assembly. *J. Supramol. Struct.* 2:202–224.

44. Hu, B., W. Margolin, …, J. Liu. 2015. Structural remodeling of bacteriophage T4 and host membranes during infection initiation. *Proc. Natl. Acad. Sci. USA.* 112:E4919–E4928.

45. Dai, W., C. Fu, …, W. Chiu. 2013. Visualizing virus assembly intermediates inside marine cyanobacteria. *Nature.* 502:707–710.

46. Farley, M. M., J. Tu, …, J. Liu. 2017. Ultrastructural analysis of bacteriophage Φ29 during infection of Bacillus subtilis. *J. Struct. Biol.* 197:163–171.

47. Lander, G. C., S. M. Stagg, …, B. Carragher. 2009. Appion: an integrated, database-driven pipeline to facilitate EM image processing. *J. Struct. Biol.* 166:95–102.

48. Tang, G., L. Peng, …, S. J. Ludtke. 2007. EMAN2: an extensible image processing suite for electron microscopy. *J. Struct. Biol.* 157:38–46.

49. Rohou, A., and N. Grigorieff. 2015. CTFFIND4: fast and accurate defocus estimation from electron micrographs. *J. Struct. Biol.* 192:216–221.

50. Lokareddy, R. K., R. S. Sankhala, …, G. Cingolani. 2017. Portal protein functions akin to a DNA-sensor that couples genome-packaging to icosahedral capsid maturation. *Nat. Commun.* 8:14310.

51. Grigorieff, N. 2016. Frealign: an exploratory tool for single-particle Cryo-EM. *Methods Enzymol.* 579:191–226.

52. Henderson, R., A. Sali, …, C. L. Lawson. 2012. Outcome of the first electron microscopy validation task force meeting. *Structure.* 20:205–214.

53. Pettersen, E. F., T. D. Goddard, …, T. E. Ferrin. 2004. UCSF Chimera–a visualization system for exploratory research and analysis. *J. Comput. Chem.* 25:1605–1612.

54. Heymann, J. B., and D. M. Belnap. 2007. Bsoft: image processing and molecular modeling for electron microscopy. *J. Struct. Biol.* 157:3–18.

55. Yan, X., R. S. Sinkovits, and T. S. Baker. 2007. AUTO3DEM–an automated and high throughput program for image reconstruction of icosahedral particles. *J. Struct. Biol.* 157:73–82.

56. Rossmann, M. G., and D. M. Blow. 1962. The detection of sub-units within the crystallographic asymmetric unit. *Acta Crystallogr.* 15:24–31.

57. Neuman, B. W., B. D. Adair, …, M. J. Buchmeier. 2006. Supramolecular architecture of severe acute respiratory syndrome coronavirus revealed by electron cryomicroscopy. *J. Virol.* 80:7918–7928.

58. Winston, F., D. Botstein, and J. H. Miller. 1979. Characterization of amber and ochre suppressors in Salmonella typhimurium. *J. Bacteriol.* 137:433–439.

59. Earnshaw, W., S. Casjens, and S. C. Harrison. 1976. Assembly of the head of bacteriophage P22: x-ray diffraction from heads, proheads and related structures. *J. Mol. Biol.* 104:387–410.

60. Suloway, C., J. Pulokas, …, B. Carragher. 2005. Automated molecular microscopy: the new Leginon system. *J. Struct. Biol.* 151:41–60.